Quasi-static chain drive model for efficiency calculation - Application to track cycling

G. Lanaspeze, Bérengère Guilbert, L. Manin, F. Ville

Mechanism and Machine Theory 203 (2024) 105780

Contents lists available at ScienceDirect

Mechanism and Machine Theory

journal homepage: www.elsevier.com/locate/mechmt

Research paper

Quasi-static chain drive model for efficiency calculation - Application to track cycling

G. Lanaspeze, B. Guilbert *, L. Manin, F. Ville

INSA Lyon, CNRS, LaMCoS, UMR5259, 69621 Villeurbanne, France

ARTICLE INFO

Keywords:
Efficiency
Track cycling
Quasi-static model

ABSTRACT

Intense competition between top-level track cycling athletes rEq.uires research to make optimisation possible. In this context, the energetic efficiency of roller chain drives is studied to improve understanding of loss sources and to propose improvements. Losses in chain drives are mainly caused by the meshing/un-meshing process of chain links on the sprockets. However, a preliminary study shows that losses caused by the motion of rollers along their associated tooth profile have a significant influence. The aim of this paper is therefore to explore this phenomenon. An original 2D quasi static model of a two-sprocket drive is presented. The global drive kinematics (including transmission error) is determined using specific sub-models for the tight and slack strands. A local sprocket sub-model is then introduced to calculate link tension, roller/sprocket contact force and roller location. This model can be used for different tooth profile geometries. Based on the results provided by the global and local model, the presented model calculates drive efficiency, considering the losses caused by meshing and roller motion. A comparison with literature is done to ensure the model validity.

1. Introduction

1.1. Cycling drive context

The chain transmission conveys the power from a motor to a receptor. The first sketches of modern chains can be traced back to Leonardo da Vinci [1]. Hans Renold invented the bush roller chain in the late 19th century [2]. The addition of bushes and rollers (Fig. 1) reduces wear and leads to a significant improvement of chain life, allowing the mechanism to be widely used [3-6]. Chains are composed of an alternance of inner and outer links (also bush and pin links, see Fig. 1). The distance between the axis of two consecutive bushes is called the chain pitch.

In bicycle applications, the chain transmits the power from the cyclist to the rear wheel. Track bicycles use single speed drives with no derailleur and fixed gear ratio as a result. The variety of races (sprint to endurance) gives a high range of operating conditions that can go up to 130 rpm or 300 N.m. Final time differences between athletes are usually very close (1/100 seconds for the Tokyo 2021 Olympic games). These reduced gaps justify the interest of chain drive optimisation as little improvements can decide the race winner. Track cycling drives are also characterised by light chains (around 3.6g) and high gear ratio (between 3 and 5). The tension is chosen to avoid chain drop during races. As a result, the centrifugal force can be neglected in front of chain tension and a quasi-static approach is

* Corresponding author.
E-mail address: berengere.guilbert@insa-lyon.fr (B. Guilbert).

https://doi.org/10.1016/j.mechmachtheory.2024.105780
Received 15 May 2024; Received in revised form 23 August 2024; Accepted 26 August 2024
Available online 3 September 2024

Nomenclature

a	[m] Transition of friction correction parameter (tanh width)
C_j	[$N.m$] Torque associated with sprocket j
d	[m] Absolute roller displacement
D_{bush}	[m] Chain bush diameter
D_{pin}	[m] Chain pin diameter
D_{roller}	[m] Chain roller diameter
$D_{x,y}$	[m] Horizontal and vertical distance between the slack strand tips
ΔX	[m] Horizontal distance between the axes of the driving and driver sprockets
ΔY	[m] Vertical distance between the axes of the driving and driver sprockets
F	[N] Generic letter for forces
f	[-] Parameter for tight strand length (from Fuglede & Thomsen [1])
L	[m] Distance between the axes of the driving and driver sprockets
M_j	[-] Tangency points for the tight strand common tangent
m_{link}	[kg] Chain link mass
$n_{j,s,t,tot}$	[-] Number of links
N_j	[-] Tangency points for the slack strand common tangent
O_j	[-] Sprocket center
$P_{loss,mesh,roller}$	[W] Dissipated powers
p	[m] Chain pitch
$P_{i,k}$	[N] Roller sprocket contact force
r	[m] Chainette parameter
$R_{1,2,etc.}$	[m] Radius of tooth profile circle arc portion
R_{curve}	[m] Local tooth profile curvature radius
R_j, R_{pitch}	[m] Pitch radius of sprocket j
R_{tb}	[m] Tooth bottom radius
$slack$	[-] Mid-span movement as a fraction of L
$T_{i,j,k,s,t}$	[N] Link tension force
T_s/T_t	[-] Tension ratio
$\mathbf{u}$	[-] Outgoing normal at roller contact with profile
$\mathbf{v}$	[-] Link direction vector
W	[J] Generic letter for mechanical work
x_t	[m] Length of the tight chain strand
Z	[-] Number of teeth
α^*	[rad] Angles between two consecutive links
α_j	[rad] Angular pitch of sprocket j
$\alpha_{s,t,j}$	[rad] Angle between a chain strand and the closest link with both rollers contacting sprocket j
β	[rad] Tilt angle of the pitch circles common tangent relatively to the centre direction
δ	[rad] Friction correction angle
$\lvert\delta(\infty)\rvert$	[rad] Correction angle outside
ε	[-] Generic displacement of each chain part between sub-positions
η	[-] Chain drive efficiency
γ	[-] Non-dimensional roller location coordinate
$\gamma_{tp}^{A,B}$	[-] Non-dimensional roller location coordinate at transition points A and B
κ	[rad] Angle between the direction of the preceding link a the local $\mathbf{x}$ axis
λ_i	[rad] Tilt angle for a slack strand link relatively to the horizontal direction
$\overline{\mu}$	[-] Global friction coefficient
μ	[-] Friction coefficient
ν	[rad] Angle between the direction of the following link a the local $\mathbf{x}$ axis
ϕ	[rad] Roller contact angle
$\psi_{s,t,j}$	[rad] Angle between a strand tip on sprocket j and the point of tangential contact
$\psi_{t,I,init}$	[rad] Initial value for angle $\psi_{t,I}$
s_c	[m] Curvilinear abscissa of the roller/profile contact point along its trajectory
s_r	[m] Curvilinear abscissa of the roller centre along its trajectory
τ	[rad] Tilt angle of the drive centre direction relatively to the horizontal
θ	[rad] Generic letter for angles
ζ	[rad] Driving sprocket rotation angle

Ω_j	$[rad/s]$ Rotation speed
Indices	
i	Rollers and links spatial numbering for kinematics
j	Sprocket numbering.
I	for the driving sprocket/chainring, II for the driven sprocket/rear cog.
m	Explored sub-positions within a drive period. Varies between 1 and nb_{pos}.
Subscripts	
A, B	Relative to kinematic cases A and B
br	Relative to Bush/Roller chain interface
$init$	Use for variables related to the starting position of the kinematic calculation ($m = 1$)
pb	Relative to Pin/Bush chain interface
rp	Relative to Roller/Profile chain interface
s	Attribute of the slack chain strand
t	Attribute of the tight chain strand
tp	Attribute of the roller location transition points
Superscripts	
k	Drive sub-position for efficiency calculation

well adapted.

1.2. Previous research works

A typical chain drive is represented in Fig. 2. The driving sprocket is at the right-hand side with index I while the driven sprocket is on the left with index II. The driving sprocket rotates clockwise. Therefore, the tight strand is the upper one and transmits loads. The slack one is at the bottom. The strand tips mark the transition between the links in the chain strands and those meshed with a sprocket (see Fig. 2).

In a first approximation, the radius difference between the roller and the tooth bottom can be neglected [7]. Thus, the centre of the rollers in contact with a sprocket lies at the vertices of the pitch polygon (in red on Fig. 2). The strand tip movement along the pitch circle causes the strand tip speed direction to vary as a consequence of the chain discrete nature. This phenomenon is denoted polygonal effect, due to the chain shape approximately following the pitch polygon. The polygonal effect induces periodical variations of the rotational speed ratio, causing transmission error.

Binder [8] was the first to propose a model of a chain drive for efficiency calculation. He considered the dependency between the rotation of the driving and driven sprockets using a four-bar mechanism. Thus, the strand tip positions move along the pitch circles, making it possible to model the polygonal effect and losses due to link meshing. He limited his study to drives with a horizontal tight strand common tangent to both pitch circles. The results show that the influence of the polygonal effect decreases as the numbers of teeth increase. He proposed expressions for power loss and introduced a distinction between pin and bush articulations each producing different power losses. Mahalingam [9] and Morrison [10] proposed similar kinematics studies and also found that multiple number of pitch case should be preferred to limit kinematic perturbations. In [11], Bouillon & Tordion tested experimentally the kinematic theory based on a four-bar mechanism. In [12-13] Fuglede & Thomsen also modelled the kinematic consequences of the polygonal effect using a four-bar mechanism. In the 1980s, Naji & Marshek [15-16] produced numerous studies aimed at improving the first approach introduced by Binder. They introduced the Geometric Progressive Load Distribution (GPLD) tension model. Sprocket orientation was considered, correcting Eq.uations for the process of meshing and un-meshing. To account for the slack strand tension, Naji & Marshek proposed that each roller can contact either the tight (Binder's approach) or the slack side of its associated tooth profile while

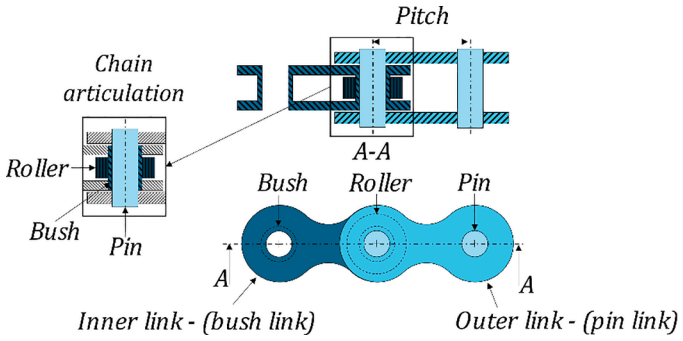

Fig. 1. Nomenclature of a modern roller chain.

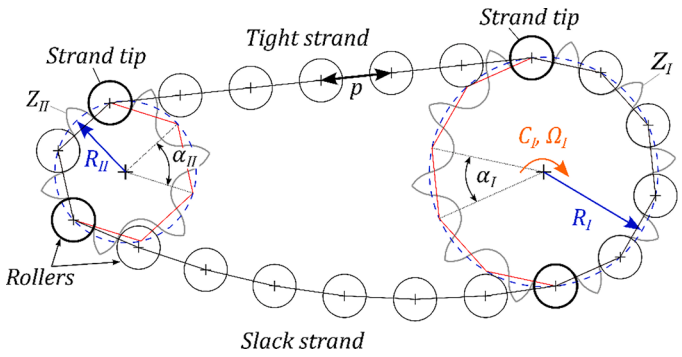

Fig. 2. Diagram of chain drive principle.

remaining seated. In following studies [17-18], they extended the possibilities of roller location along its associated tooth profile, applying the new approach only to un-seated rollers. This model was used to assess the influence of pin link elongation due to wear. Hollingworth & Hills [19-20] proposed a study of chain drive efficiency dedicated to cranked link chains. They assumed that only link meshing contributes to chain drive power losses. Coulomb friction was assumed at all chain interfaces. The results showed that pin articulation should be favoured for drives such that $Z_{II} > Z_I$. However, the proposed power loss expressions could not be derived by the author. Later, Kim & Johnson [21] completed the process and proposed a link tension model with full dependency between roller location and loads. This allowed locating the roller at any curve portion even when contacting the tooth bottom. Verne [22] applied the full roller location methodology of Kim & Johnson to the GPLD model. This model was then applied to entire drives (*i.e.*, not only for one sprocket) but strand tensions were still assumed. Contrary to Naji & Marshek, both link elongation and tooth deflection were considered. Troedsson & Vedmar proposed static and dynamic drive models [23-24]. The full roller location approach of Kim & Johnson was also used [21]. Link elongation was considered but tooth deflection was neglected. Moreover, Troedsson and Vedmar introduced a specific sub-model for the slack strand. Thanks to this new component, the dependency between sprockets was introduced. Therefore, a single resolution was carried out for the entire drive but numerical challenges associated with this resolution [25] were reported. Multibody dynamic models were also proposed [26–31] and in [32,33] Omar proposed a multibody formulation to study bicycle chain drive dynamics including the derailleur system. Example of link tension and acceleration were given. The question of the dynamical behaviour is mainly addressed in industrial applications where high rotational speeds (thousands of rpm can be reached) makes it more likely to encounter natural frequencies and therefore trigger significant vibrations.

In the cycling field, Kidd [34] proposed a quasi-static efficiency model where meshing losses were considered with distinction between pin and bush articulations. Potential drive misalignments were also modelled. The analysis of each sprocket contribution to losses highlighted the dominant contribution of the rear cog. This higher contribution was attributed to the smaller number of rear cog teeth encountered in usual cycling drives. Lodge & Burgess proposed a different approach in [35-37] to investigate cycling and industrial drives. Indeed, in their study, roller location was not relevant and they opted for a less computationally intensive study. Instead of using full roller location, they proposed three sub-models meant to represent three possible sprocket behaviours. An efficiency model was derived which assumed meshing losses to be the only source of losses. The distinction between pin and bush articulation was considered. The dissipated work was calculated by integrating the loads given by each sub-model. The model proposed was able to capture the increasing efficiency for rising torque as well as the interest of larger sprockets. However, discrepancies between the model and the experimental measurements were reported for low torque and heavy chains. These differences were attributed to neglected loss phenomena such as vibrations and impacts between rollers and sprockets. Spicer [38] proposed an analytical model of bicycle chain drive efficiency, including the effect of the derailleur system and induced chain shift. A formula for losses due to roller movement has also been proposed, which takes into account the movement of the rollers during the meshing and unmeshing of the links. However, previous tension models including the use of roller location, such as those by Troedsson, Kim and Verne mentioned above, show the importance of roller movement out of meshing and unmeshing area. Later, based on these works, a rough attempt was made [39] to consider the contribution of losses caused by roller motion along the corresponding tooth profile during the full cycle (not only meshing and un-meshing). This type of loss was denoted roller losses. The results suggested that roller losses could be as influential as meshing losses and a conclusion was drawn on the necessity to include them with a more representative model.

The objective of this paper is to present the Chain Drive Efficiency Model (CDEM) dedicated to chain drive efficiency study which takes into account the influence of losses caused by roller motion along the associated tooth profile. The model will be able to consider different tooth profiles which will be used to test the influence of various parameters on drive efficiency.

Efficiency modelling will be carried out in two steps. First an original quasi-static chain drive model will be presented. Compared to previous works, its formulation is general such that any tooth profile geometry can be considered. This first model will compute loads (*i.e.*, link tension and roller/sprocket contact force) and displacements (*i.e.*, roller motion and link orientation). Elements of previous studies by Lodge & Burgess [35], Troedsson & Vedmar [25] and Kim & Johnson [21] will be reused. An original architecture based on dedicated sub-models for chain strands and sprocket is proposed to facilitate the numerical resolution and therefore limit the possible issues reported by Troedsson & Vedmar [25]. A validation will be presented from experimental data of the literature [35], which are

based on industrial drives.

2. CDEM kinematics and load calculation

2.1. Chain drive efficiency model (CDEM) modelling strategy

The CDEM model assumes that all bodies are rigid. This hypothesis is not very restrictive in the context of single speed cycling as the drives are usually set with non-negligible tension in the slack strand which significantly constrains its trajectory. Moreover, as bicycle chains are usually relatively light (≈3,6g / link), and with low rotational speed (150rpm on the chainring at most), dynamic effects are considered negligible. Thus, the presented model is quasi-static, and is therefore not subject to any speed or inertia effects. Due to the lightness of the chain in relation to the loads applied, the effect of gravity is not taken into account, except in the soft strand model which will be described in the overall kinematics (part 2.2). Both sprockets are assumed to be perfectly aligned and their pitch are identical to the chain pitch (denoted p). The kinematics is considered independent from the loads and only the global motions of the bodies are modelled. Therefore, backlashes, as well as relative motions between each roller and its corresponding tooth profile are neglected. Consequently, the centre of every roller in contact with a sprocket is assumed to lie on the pitch circle. Finally, the effect of gravitation is also neglected with regard to the loads involved.

The modelling strategy is divided into three main steps (Fig. 3). First, the drive kinematics is established (i.e. the location of each components) for a given set of drive positions. Then, loads are calculated depending on the determined locations. Finally, the efficiency is computed from the local sub-model results and loading conditions.

The driving and driven sprockets are denoted $j = I$ and $J = II$, respectively (see Fig. 1). The number of links with both rollers in contact with the driving and the driven sprockets are denoted n_I and n_{II}, respectively. The number of links in the tight and slack strand are n_t and n_s, respectively. Therefore, the total number of links and rollers in the chain n_{tot} is given by Eq.(1).

$$n_{tot} = n_I + n_{II} + n_s + n_t \tag{1}$$

The spatial index of articulation (roller + preceding link in rotation direction) is denoted i on the geometry with $i = 1$ the first roller in contact with the driving sprocket and increasing in rotation direction. k position step and represent the evolution of one component going through all the possible i during drive rotation.

For the global kinematics, the clearance between the roller and the tooth profile is neglected. Therefore, it is assumed that the centres of the rollers in contact with a sprocket lie on the corresponding pitch circle. Based on [7], Fig. 4 shows the parameters used to characterise a given drive.

The parameters in Fig. 4 are:

- $\alpha_j = 2\pi/Z_j$, the angular pitch of sprocket j. Z_j being the number of teeth of sprocket j
- p, the chain and sprocket pitch (assumed to be equal),
- $L = \| \mathbf{O_{II}O_I} \|$, the centre distance between the driving and driven sprocket axes,
- $\tau = (\mathbf{x}, \mathbf{O_{II}O_I})$, the tilting angle between the centre axis $\mathbf{O_{II}O_I}$ and the horizontal direction $\mathbf{x}$,
- $\Delta Y = \mathbf{O_IO_{II}}.\mathbf{y}$, the vertical signed distance between the sprocket axes,
- $\Delta X = \mathbf{O_{II}O_I}.\mathbf{x}$, the horizontal signed distance between the sprocket axes,
- $R_j = p/\left[\sin(\alpha_j/2)\right]$, the radius of the pitch circle for sprocket j,
- $\beta = (\mathbf{O_{II}O_I}, \mathbf{M_{II}M_I})$, the angle between the centre axis $\mathbf{O_{II}O_I}$ and the top common tangent.

2.2. Global kinematics

As the tight strand is assumed to be straight, the tension is the same for all the included links. This particularly stands for the boundary link tensions T_i and $T_{i+n_I+n_s+n_{II}+1}$ denoted $T_{t,I}$ and $T_{t,II}$ respectively (see Eq.(2), link numbering is given in (1)). The angles are defined in [39].

$$T_{t,I} = T_{i=1} = T_{n_I+n_s+n_{II}+2} = T_{t,II} \tag{2}$$

As with the tight strand, the slack strand tips are the centres of the first and last contacting rollers of the driven and the driving

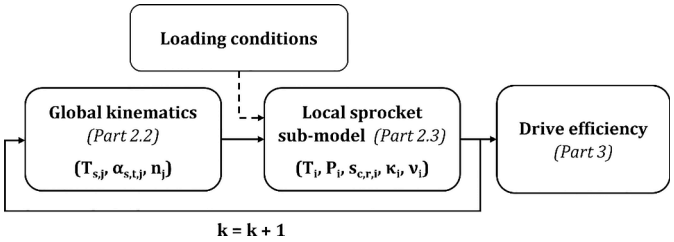

Fig. 3. Algorithm of the chain drive efficiency model (CDEM), with associated publication parts

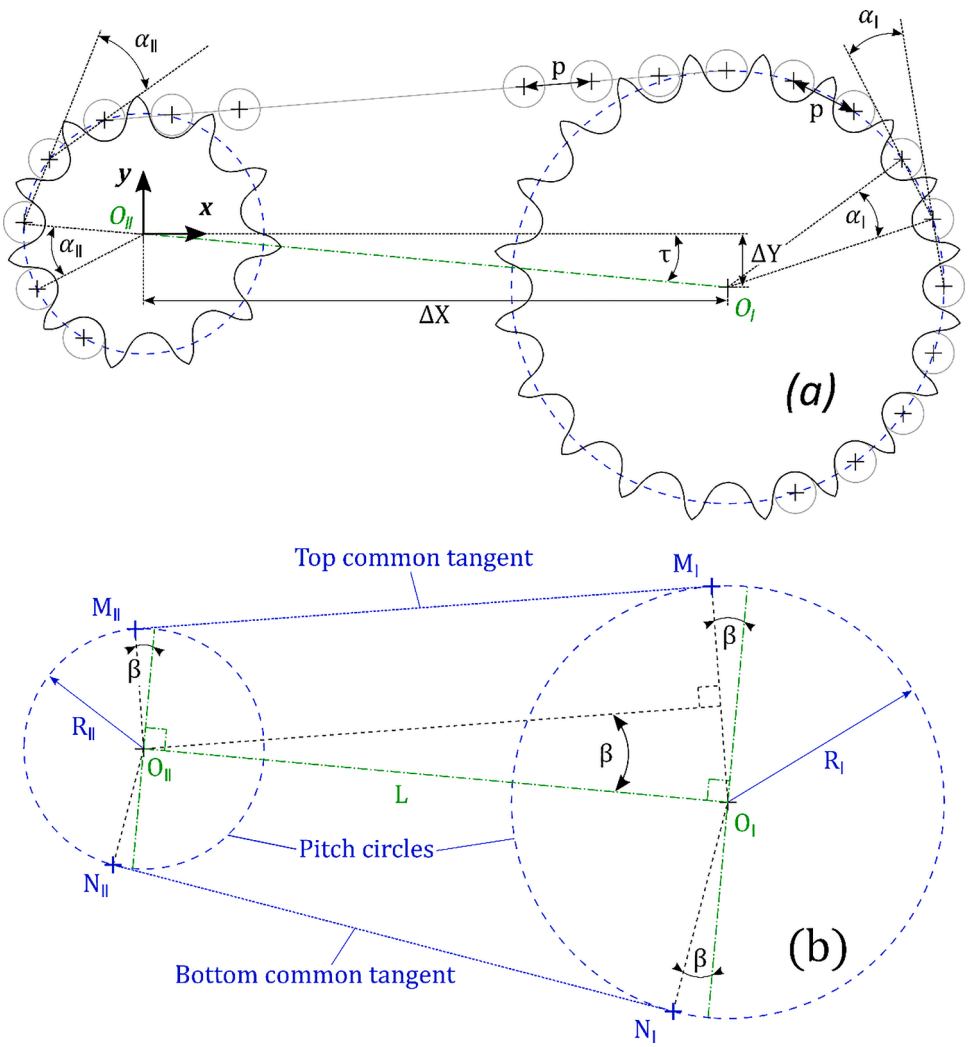

Fig. 4. Drive geometry with a) drive parameters and b) pitch circles and common tangents.

sprockets, respectively. Their roller centres are designated as E_j and the centres of the adjacent rollers are D_j and F_j (see Fig. 5).

Angles $\alpha_{s,j}$ (Fig. 5) and $\psi_{s,j}$ (Fig. 6) are also defined in a similar way to the tight strand in Eq.(3).

$$\begin{aligned}\alpha_{s,j} &= \left(\mathbf{E_jF_j}, \mathbf{D_jE_j}\right)\\ \psi_{s,j} &= \left(\mathbf{O_jN_j}, \mathbf{O_jE_j}\right)\end{aligned} \tag{3}$$

With $j = I, II$ depending on driving or driven sprocket.

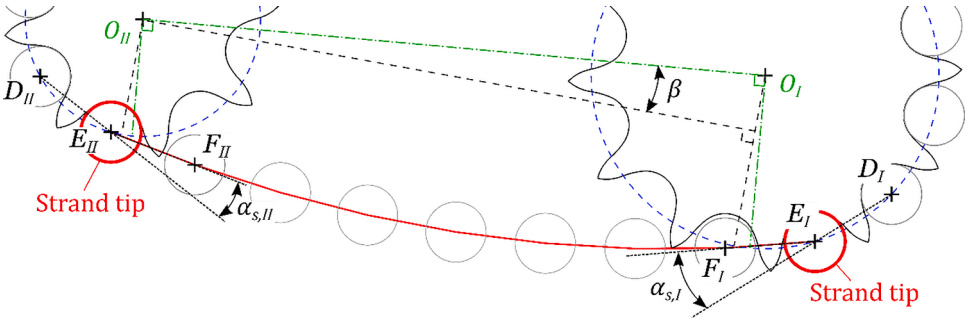

Fig. 5. Slack strand definition.

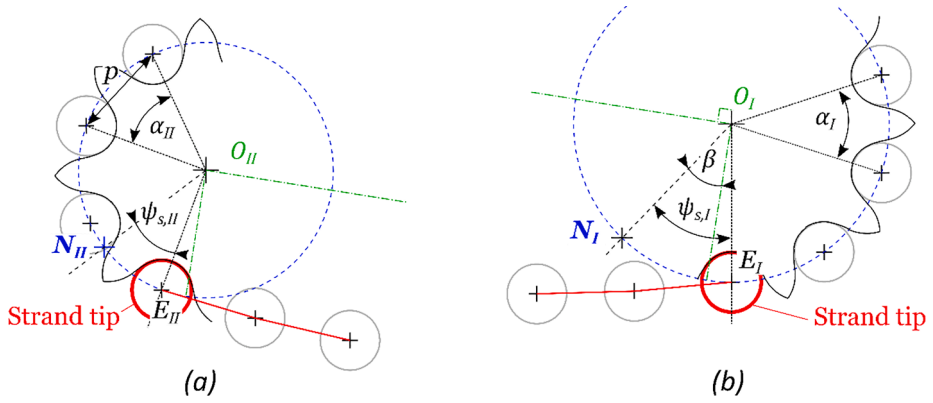

Fig. 6. Definition of a) $\psi_{s,II}$ and b) $\psi_{s,I}$.

As the slack strand does not transmit load, its tension is significantly lower than the tight one. As such, the effect of gravity on the strand trajectory is preponderant. To consider this effect, the model presented by Troedsson & Vedmar [23] and improved by Lodge & Burgess [35] is used. The load in the strand is assumed to be due solely to gravitation and the link masses are considered to be lumped at the roller centres. The slack strand is therefore modelled as a set of punctual masses (each with mass m_{link}) linked with massless bars (see Fig. 7). The centre of roller i is designated as R_i.

A given roller is subjected to three external forces (Fig. 7). The tension in the preceding and following links (respectively T_i and T_{i+1}) and the weight (corresponding to the weight of one chain link of mass m_{link}). The spatial direction of link i is given relatively to the horizontal direction (**x** in Fig. 7) by angle λ_i. The equilibrium of a roller leads to the following equation.

$$T_{i+1} = T_i \frac{\cos(\lambda_i)}{\cos(\lambda_{i+1})} \tag{4}$$

With: $\tan(\lambda_{i+1}) = \frac{m_{link}g + T_i \sin(\lambda_i)}{T_i \cos(\lambda_i)}$ and $\lambda_i = (\mathbf{x}, \mathbf{R_i R_{i-1}})$

Eq. (4) connects the characteristics of one roller/link pair (*e.g.*, λ_i and T_i) with the following one (λ_{i+1}, T_{i+1}). Therefore, if a set of values (T_i, λ_i) is known, it is possible to calculate all the tensions and link orientations considering all the rollers step by step.

Moreover, as presented by Lodge & Burgess in [35], a valid slack strand must fulfil the following Equations (Eq.. (5), see Fig. 7), ensuring that a set of angles λ_i is consistent with the positions of the strand boundaries.

$$\begin{aligned} \sum_{i=n_l+2}^{n_l+n_s+1} p\cos(\lambda_i) - D_x = 0 \\ \sum_{i=n_l+2}^{n_l+n_s+1} p\sin(\lambda_i) - D_y = 0 \end{aligned} \tag{5}$$

Therefore, once the slack strand tips' locations are known (*i.e.*, angles $\psi_{s,j}$), distances D_x and D_y are deduced and the corresponding slack strand can be calculated. Numerical search is used to find a set of values (*e.g.*, T_{n_l+2}, λ_{n_l+2}) resulting in the smallest residual value on Eq. (5). Similarly with the tight strand, once the slack strand trajectory is known (angles λ_i for all rollers), the values of angles $\alpha_{s,I}$ and $\alpha_{s,II}$ can be computed using Eq. (3).

The tension in the boundary links ($T_{i=n_l+2}$ and $T_{i=n_l+n_s+1}$) are denoted $T_{s,I}$ and $T_{s,II}$, respectively. Unlike the tight strand, they do not necessarily have the same value [39].

$$T_{s,I} = T_{i=n_l+2} = T_{i=n_l+n_s+n_t} = T_{s,II} \tag{6}$$

The slack strand sub-model can only be used in conditions where the number of links in the strand is sufficient. As no link

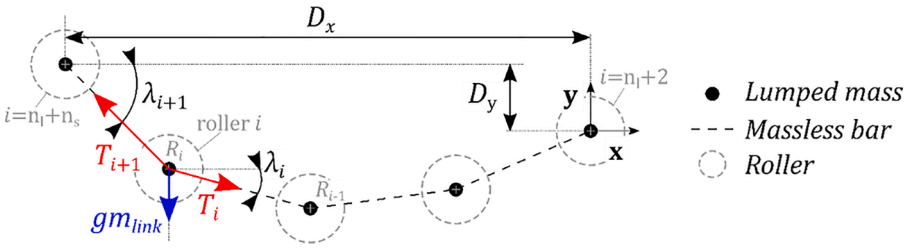

Fig. 7. Slack strand model.

elongation is modelled, the condition translates in Eq. (7), ensuring that the distance between strand tips is smaller than the strand length.

$$\sqrt{D_x^2 + D_y^2} < pn_s \tag{7}$$

In order to study the influence of the tension setting on drive behaviour and efficiency, it is necessary to quantify strand looseness. A representation of the chain tension is usually obtained with a measure of the mid-span movement (*i.e.*, the peak to peak slack strand deflection) expressed as a proportion of L [40] (Fig. 8). The mid-span recommendation is 4-6% of L for regular industrial drives [40]. For sensitive transmissions (high speed, impulse, reversing) the setting can be reduced to 2-3% [40].

The procedure to geometrically calculate the mid-span movement for a given drive sub-position is given in the appendix A. As its value changes for each sub-position (*i.e.*, for each driving sprocket orientation), the looseness setting of a given drive is calculated as the mean mid-span movement value on ten linearly spaced sub-positions within the drive movement studied. For the rest of the manuscript, the looseness setting will be given as a proportion of L expressed in % for each drive studied.

The slack strand sub-model is compared to the known catenary results for hanging cables [41]. Then the prediction in terms of link orientation and tension are analysed. The catenary (or chainette) result is an analytical solution known in the literature for hanging cables subjected only to gravitational field and with continuous mass distribution.

Differences between the slack strand model presented (with discreet mass distribution) and the corresponding catenary are shown in Fig. 9. As the results are independent of the scale of the chain, they are given relatively to the chain pitch p (scaled variables are given with a bar, e.g., $\overline{X} = X/p$). The link mass and roller diameter are given for a standard track cycling chain ($p = 12.7mm$; $m_{link} = 3.6g$; $D_{roller} = 7.75mm$).

Both models show the same trend. The trajectories obtained exhibit a bell shape tending toward a straight line as the distance between the tips increases. Comparisons with the catenary curve show notable differences for small x spans. In Fig. 9.a, the small number of links in the strand results in sharp changes in link orientation, causing considerable deviation from the smooth catenary curve. For values of $\overline{D}_x$ and $\overline{D}_y$ more compatible with a real chain strand (Fig. 9.b), the difference becomes negligible. The discreet approach used in the model presented therefore shows greater interest for strands with a high number of links (longer chain) and small spans. The resulting model of the transmission kinematics is solved with a step-by-step algorithm described in [39].

2.3. Local geometry, load calculation

2.3.1. Local geometry definition

In this model, it is assumed that all sprocket angular sectors are identical. Therefore, a sprocket is fully defined by one angular sector in the local coordinate system $(O_i, \mathbf{x_i}, \mathbf{y_i})$ (see Fig. 10.b). The angular sector is defined as a piecewise curve where each portion is either a circle arc or a straight line. The definition of the portions must ensure the continuity of the slope (*i.e.,* the derivative of the curve). Moreover, the defined geometry must be such that it is not possible for a roller to contact the profile at more than one point. This implies that the radius of any convex circle portion (especially the tooth bottom circle of radius R_{tb}) must be greater than the roller radius (*e.g.*, $R_{tb} > R_{roller}$ in Fig. 10.b).

Axes $\mathbf{x_i}$ and $\mathbf{y_i}$ can be seen in the radial and tangential directions to the pitch circle at the local origin respectively (see Fig. 10.b). The local origins of two adjacent tooth profiles are α_j apart.

Knowing the roller radius and the definition of the tooth profile, it is possible to determine the roller centre trajectory. This curve is composed of all the possible locations for the centre of a roller in contact with the defined profile. In practice, this curve is defined as the parallel to the tooth profile (toward O_i), shifted by R_{roller} (Fig. 10). It therefore has the same number of circle arcs and lines as the tooth profile.

To locate the roller along its corresponding tooth profile, three different coordinates are used (see Fig. 10.a). These three coordinates are intertwined and knowing only one of them is sufficient to calculate the remaining two.

- γ is a dimensionless coordinate. The definition is similar to coordinates η and ξ in [23] and [20] respectively. γ starts at 0 and is an integer at each point of transition between two portions of the curve. Therefore, γ ranges between $[0, Nb_{portion}]$, with $Nb_{portion}$ being

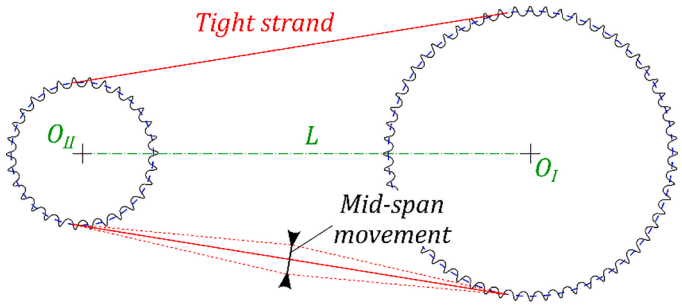

Fig. 8. Mid-span movement of the slack strand, adapted from [40].

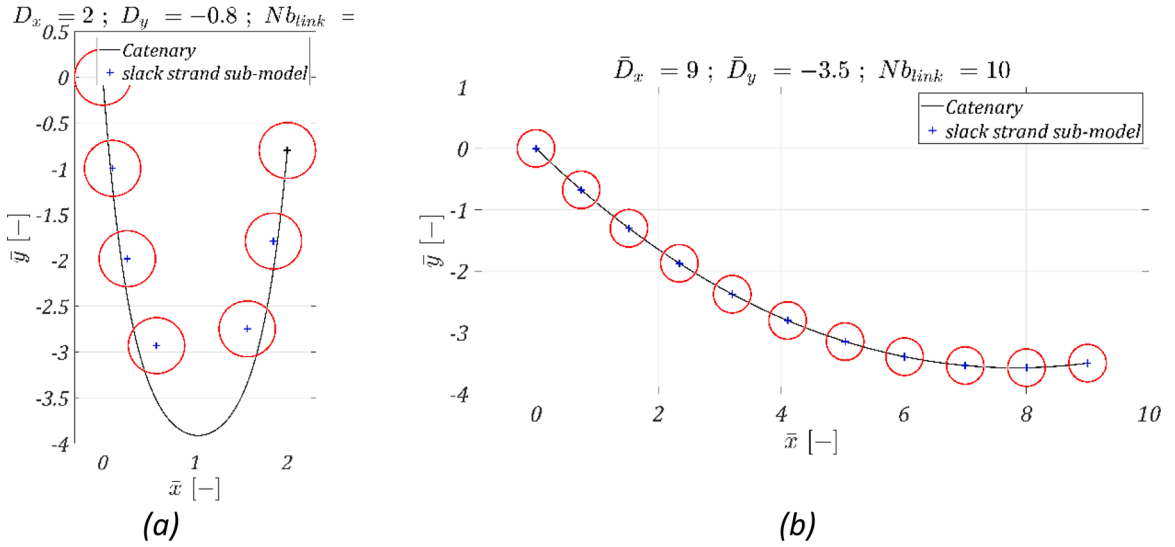

Fig. 9. Comparisons between the slack strand sub-model and the catenary curve (a) $\bar{D}_x = 2$, $\bar{D}_y = -0.8$, $n_s = 6$ (b) $\bar{D}_x = 9$,$\bar{D}_y = -3.5$,$n_s = 10$ with$\bar{m}_{link} = 0.28g/m$; $\bar{D}_{roller} = 0.61$.

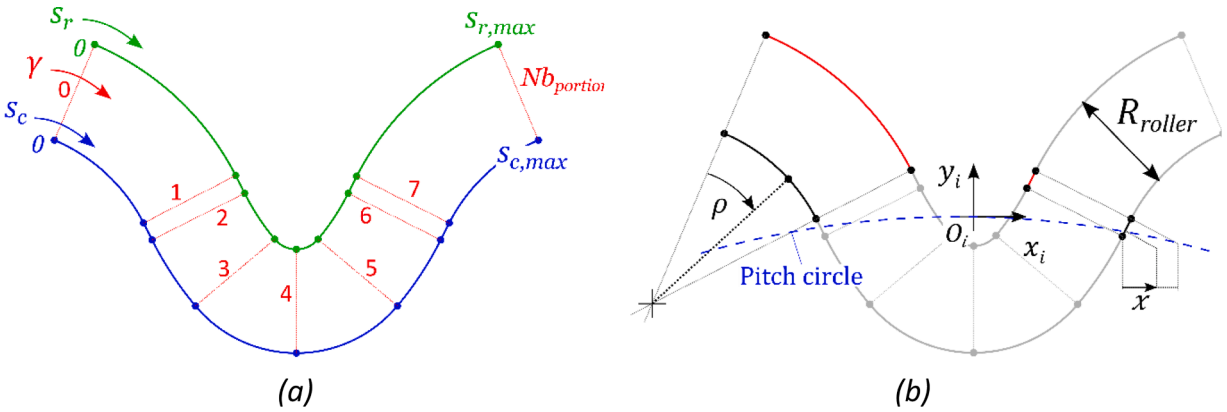

Fig. 10. (a) Roller location coordinates (b) Definition of circle arc and line profile portion (the clearance between roller and profile is exaggerated).

the number of curve portions defining the tooth profile. Between integers, γ varies linearly with the sweeping angle θ for circle sectors and with x for the straight parts (see Fig. 10.b).

- s_c is the curvilinear abscissa of the contact point between the roller and its corresponding tooth profile (along the tooth profile).
- s_r is the curvilinear abscissa of the roller centre along the roller centre trajectory.

Coordinate γ is easier to interpret than the curvilinear abscissas but it also distorts reality. A distance of *e.g.*, $\Delta\gamma = 0.5$ does not correspond to the same distance in *mm* depending on the curve portion considered. On the contrary, the curvilinear abscissas will be used for calculations but their interpretation in terms of roller position along the tooth profile is more difficult.

2.3.2. Relation between consecutive roller locations

The relation between consecutive roller locations is considered in a way similar to [21,23]. Therefore, adjacent rollers on a given sprocket are distant by a chain pitch p. Knowing the location of a roller, the adjacent one will lie on the roller centre trajectory of the adjacent profile at a distance p. The problem can then be treated as finding the intersection between a circle of radius p centred at the known roller position and the adjacent roller centre trajectory.

2.3.3. Angles between links

Depending on the location of each roller along its corresponding tooth profile (represented by coordinate γ), the relative position of consecutive links is not the same. However, these positions will prove useful to link roller locations to loading conditions and later to calculate the efficiency of a chain drive and must therefore be tracked.

To do so, four angles are defined for each roller (Fig. 11):

- $\alpha_i^* = (\mathbf{R_i R_{i+1}}, \mathbf{R_{i-1} R_i})$, angle between the directions of the following and preceding link (link $i+1$ and i respectively). This angle equals α if the three roller centres lie on the pitch circle as assumed for the global kinematics.
- $\phi_i = (\mathbf{R_{i-1} R_i}, \mathbf{u})$, angle between the direction of the preceding link (link i) and the profile normal at the contact point between the roller and the profile.
- $\kappa_i = (\mathbf{R_i R_{i-1}}, \mathbf{x_i})$, angle between the direction of the preceding link (link i) and the $\mathbf{x_i}$ direction in the local profile axis system.
- $\nu_i = (\mathbf{R_i R_{i+1}}, \mathbf{x_i})$, angle between the direction of the following link (link $i+1$) and the $\mathbf{x_i}$ direction in the local profile axis system.

Parameters in Fig. 11 are:

- $\mathbf{u}$, the outgoing normal at the contact point between tooth profile and roller i
- R_i, the centre of roller i

Moreover, angles κ, ν and α^* are connected by Eq. (8) (Fig. 11.c).

$$\kappa_i - \nu_i = \pi - \alpha_i^* \tag{8}$$

At this point, compatibility issues arise at the interfaces between the global kinematics (used to calculate angles $\alpha_{t,s,j}$) and the local sprocket sub-model. Indeed, for the global kinematics, all roller centres are assumed to lie on their related pitch circle while the local sprocket sub-model locates the rollers more accurately (using coordinate γ). Questions arise especially for angles α_1^*, α_{n+1}^*, κ_1, ν_{n+1} and ϕ_1 (with n being the number of links in contact with the sprocket considered). Calculating them involves the location of rollers both in a chain strand (whose trajectory is determined using the global kinematics) and in contact with the sprocket considered. These compatibility issues are represented Fig. 12. The roller location as assumed in the global kinematics calculation is represented in Fig. 12.a while the precise roller location allowed by the local sprocket sub-model is represented in Fig. 12.b.

Compatibility is solved using the following hypotheses. It is first assumed that angles α_1^*. and α_{n+1}^* are equal to angles α_t and α_s, respectively, as calculated through the global kinematic study.

$$\begin{aligned} \alpha_1^* &= \alpha_t \\ \alpha_{n+1}^* &= \alpha_s \end{aligned} \tag{9}$$

For angles κ_1 and ν_{n+1}, equation (8) is considered to be fulfilled, therefore, the angles are calculated from ν_1 and κ_{n+1}, respectively, as follows (Eq. (10)).

$$\begin{aligned} \kappa_1 &= \pi - \alpha_1^* + \nu_1 = \pi - \alpha_t + \nu_1 \\ \nu_{n+1} &= \kappa_{n+1} - \pi + \alpha_{n+1}^* = \kappa_{n+1} - \pi + \alpha_s \end{aligned} \tag{10}$$

The tight strand span is significantly larger than the roller/profile clearance (*i.e.*, $L\cos(\beta) \gg R_{tb} - R_{roller}$, with R_{tb} tooth bottom radius, curve radius in its central part). Therefore, it is assumed that the tight strand direction calculated in the global kinematics is not affected by the roller/profile clearance. Therefore, ϕ_1 is calculated using the following relation (see Fig. 13).

$$\phi_1 = \theta - \alpha_t \tag{11}$$

with: $\theta = (\mathbf{v}, \mathbf{u})$, vector $\mathbf{v} = \mathbf{O_2 O_1}$ gives the direction of link 2 and vector $\mathbf{u}$ is the outgoing profile normal at the roller profile contact point (Fig. 12).

The assumptions stated to solve the compatibility issue (Eqs. (9) to (11)) are justified by the small roller/profile clearance in real cases (about 4.3% between R_{roller} and R_{tb} for NF_{max} profile - with $D_{roller} = 7.75mm$ which gives $R_{tb} = 4.05mm$). For specific drives with a bigger roller/profile clearance, these assumptions might have more influence.

The values of all the link angles are directly related to the roller locations, themselves directly related to the location of one roller. Therefore, all the link angle values can be calculated from the location of one roller in contact with the sprocket considered.

All the parameters introduced to locate the rollers and describe their relative orientations are now used to express the Eq.uilibrium conditions of a chain in contact with a given sprocket. This results in a relation between roller locations, loads (link tension and roller-profile contact force) and external loading conditions (*e.g.*, strand tensions).

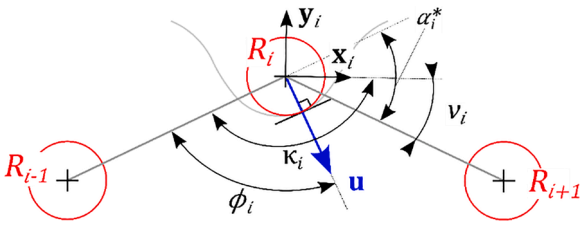

Fig. 11. Angles between consecutive links ϕ_i α_i^*, ν_i and κ_i.

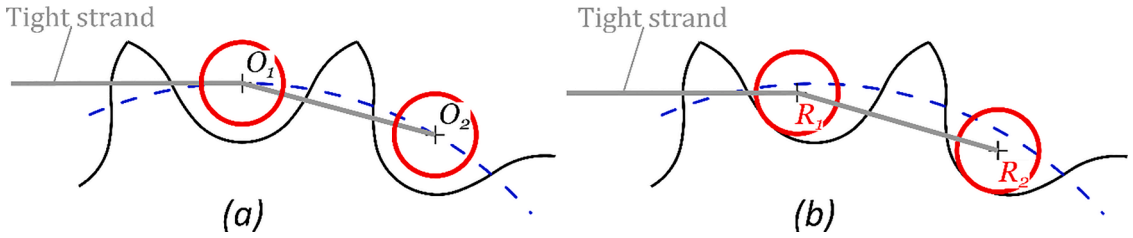

Fig. 12. Roller locations according to (a) global kinematics (b) local sprocket sub-model (the clearance between roller and profile is amplified).

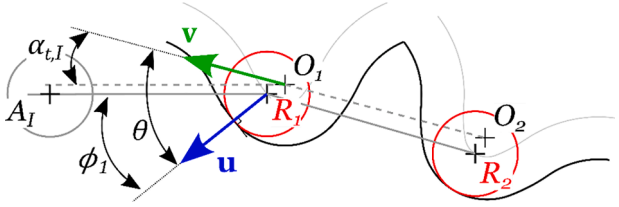

Fig. 13. Calculation of ϕ_1 (the clearance between roller and profile is exaggerated).

As with previous tension models [14,8] and [35], the equilibrium of a chain articulation (*i.e.*, a set of pin, bush and roller) is considered. The effect of gravity is neglected with respect to the other forces considered. Therefore, a chain articulation with its roller in contact with a sprocket is subjected to three external forces (Fig. 14):

- T_i, the tension force in the preceding link,
- T_{i+1}, the tension force in the following link,
- P_i, the total (*i.e.*, tangential plus normal) contact force between the roller of articulation i and its corresponding tooth profile.

It is assumed that the tension forces act along the direction of their related link. Contact force P_i acts along a roller radius and its direction is given by angle ϕ_i. As with the approach of Kim & Johnson [21] and Verne [22], angles ϕ_i and α_i^* are not assumed but calculated from the locations of rollers along their associated tooth profile.

The three forces are concurrent at the roller centre; therefore, the torque equilibrium is always verified. The equilibrium along the two planar directions (**x** and **y** in Fig. 14) leads to the following relations. These relations are similar to [8,39].

$$T_{i+1} = T_i \frac{\sin(\phi_i)}{\sin(\phi_i + \alpha_i^*)}$$
$$P_i = T_i \frac{\sin(\alpha_i^*)}{\sin(\phi_i + \alpha_i^*)} \tag{12}$$

Friction is introduced in the model in a similar way to that presented by [14]. According to this method, also used in [27,39,42-43], the moment induced by the tangential friction force (F_i in Fig. 15) is neglected. The effect of friction is therefore Eq.uivalent to a correction of the angle ϕ_i by a factor δ (Fig. 15). Angle δ is calculated based on μ_δ representing the static friction coefficient at the roller/tooth interface [14].

In the original formulation [14], the value of the correction angle had only two possibilities; $\delta = +\text{atan}(\mu_\delta)$ and $\delta = -\text{atan}(\mu_\delta)$ with no intermediate values. The correction sign must be such that the tangential friction force (F_i in Fig. 15) opposes the roller motion along its corresponding tooth profile. Consequently, this sign depends on the direction of roller motion and the sprocket studied being

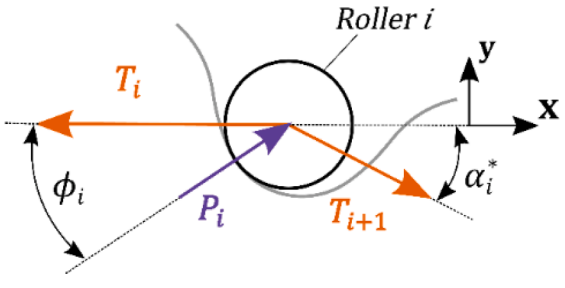

Fig. 14. Equilibrium of a chain articulation in contact with a sprocket.

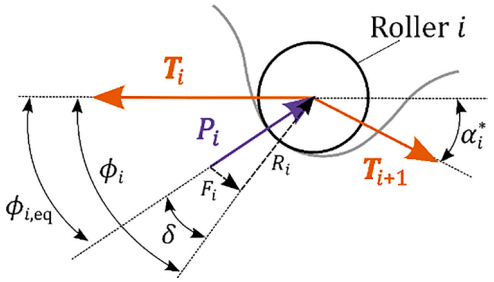

Fig. 15. Articulation Equilibrium with friction.

driving or driven [14,35]. In this model, the same principle is used. However, the correction factor can now range between $[-\text{atan}(\mu_\delta)\ , +\text{atan}(\mu_\delta)]$ as a tanh type function is used to connect the two extreme values. Moreover, it is assumed that all the rollers have the same correction angle δ and that its value is related only to the position of the first roller in contact with the sprocket considered (γ_1 or equivalently $s_{c,1}$). The sign switches at the transition point $s_{c,tp}$ as it marks the transition between zone 2 and zone 3 (see Fig. 10.a) where the direction of roller motion along the tooth profile changes (from one transition point to the other in zone 2 and toward the tooth tip in zone 3). The correction angle is therefore calculated as follows.

$$\delta(s_{c,1}) = (-1)^j \text{arctan}(\mu_\delta)\text{tanh}\left(\frac{3(s_{c,1} - s_{c,tp})}{a}\right) \tag{13}$$

The width of the tanh function is characterised by the parameter a (see Eq. (13)) such that the transition between the two extreme values $\pm\text{atan}(\mu_\delta)$ occurs between $\pm a$ according to Eq. (14).

$$\begin{aligned}\delta(a) &= 0.99\text{arctan}(\mu_\delta)\\ \delta(-a) &= -0.99\text{arctan}(\mu_\delta)\end{aligned} \tag{14}$$

Since a is a numerical parameter, its value has therefore been chosen to avoid interferences with the results. A sensitivity study was carried out and a value of $a = 1e^{-10}m$ chosen for this work (details are given in appendix B).

Adding the influence of friction to Eq. (12) leads to the new articulation equilibrium relation expressed in Eq. (15).

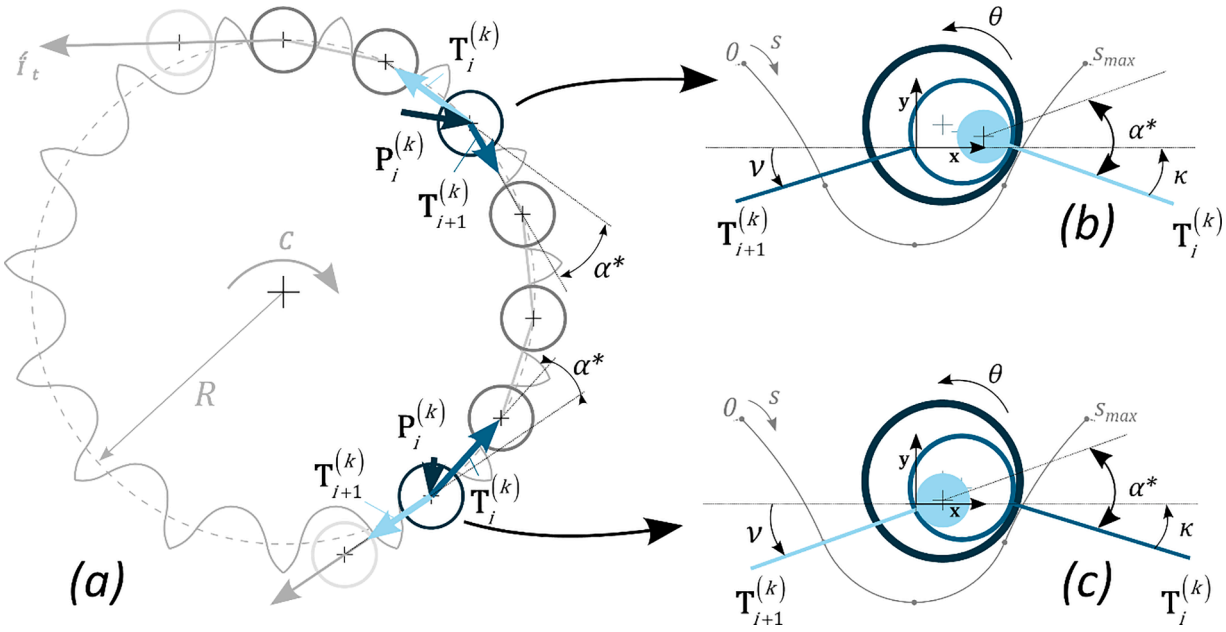

Fig. 16. (a) Loads applied on pin and bush articulations, (b) displacement parameters for pin articulation, (c) displacement parameters for bush articulation.

$$T_{i+1} = T_i \frac{\sin(\phi_i + \delta)}{\sin(\phi_i + \delta + \alpha_i^*)}$$
$$P_i = T_i \frac{\sin(\alpha_i^*)}{\sin(\phi_i + \delta + \alpha_i^*)} \tag{15}$$

Finally, the ratio between the tight and slack strand tensions is expressed in Eq. (16) considering the consecutive equilibrium of all the articulations in contact with the sprocket.

$$\frac{T_s}{T_t} = \prod_{i=1}^{n+1} \frac{\sin(\phi_i + \delta)}{\sin(\phi_i + \delta + \alpha_i^*)} \tag{16}$$

Eq. (16) highlights the direct relation between the tension ratio (ratio of the slack to tight strand tension) and angles ϕ_i and α_i^*; themself directly related to the location of one roller. Thus, the position of one roller is directly related to the tension ratio.

3. Efficiency computation

For the following development, a chain drive articulation is considered (*i.e.*, set of pin, bush and roller, see Fig. 16**.** All input variables are given per component using index k as superscript for efficiency calculation.

The following parameters are taken from the chain drive model (see Fig. 16).

- $P^{(k)}$, the contact force between the profile and the roller of the articulation considered
- $T_i^{(k)}$ and $T_{i+1}^{(k)}$, the tensions in the link preceding and following the articulation considered, respectively.
- κ, the tilting angle of the previous link (with respect to the local **x** axis);
- ν, the tilting angle of the following link (with respect to the local **x** axis);
- α^*, the angle between the following and the previous link;
- s_c, the curvilinear abscissa of the contact point between the roller and the tooth profile. To simplify notations, s_c is simply denoted s in this paper.

Although connected by Eq. (10), α^*, ν and κ are all used in the following development to facilitate understanding.

3.1. Part motion and applied load

The motions of each chain part are defined by variables s_c, α^*, κ and roller rotation angle θ (see Fig. 16b-c). Except for roller rotation, the displacement of each chain part between sub-positions k and $k+1$ is given directly according to Eq. (17).

$$\Delta\varepsilon = \varepsilon_{k+1} - \varepsilon_k \tag{17}$$

With $\varepsilon = s, \alpha^*, \nu, \kappa$.

The chain drive model proposed in this paper gives the location of the contact point between the roller and its corresponding tooth profile using variable s. However, no information is given about the rotation of the roller itself (angle θ in Fig. 16.b-c). This rotation must therefore be calculated providing kinematic hypotheses at the roller/profile contact.

Because of the complexity of the joint (pin, bush and roller), its behaviour under operating conditions is very difficult to study. As a result, the precise movement of each part remains unknown. The lubrication conditions (sliding speeds, load, film thickness, complete interface film, etc.) have not been determined. Hypothesis is made that the materials and lubrication conditions are likely to be similar at both the roller/profile and the bush/roller interfaces. However, the radius at the bush roller interface is smaller than at the roller/profile one (*e.g.*, $D_{roller} = 7.75mm$ and $D_{bush} = 5.1mm$ for usual track cycling chain). Therefore, for a given torque, sliding will occur first at the bush/roller interface. Consequently, the bush/roller interface cannot undergo rolling if the roller/profile interface is subjected to sliding. In order to assess the influence of the lubrication conditions, two extreme kinematic cases are considered called Case A and B and defined as follow.

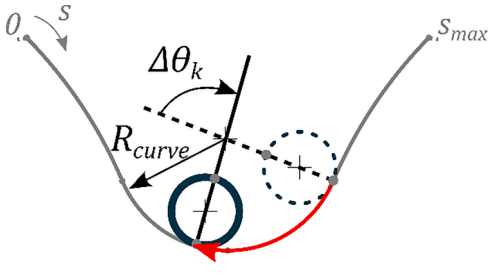

Fig. 17. Case b, sliding scheme.

Case A assumes that there is no sliding at the bush/roller interface. Therefore, the roller rolls without sliding on the tooth profile. This condition is sufficient to define roller rotation and therefore sliding occurs at the bush/roller interface. For this case, the roller kinematics implies the following equation between $\Delta\theta_k$ and Δs_k.

$$\Delta\theta_k = \frac{-\Delta s_k}{R_{roller}} \tag{18}$$

Case B assumes sliding to occur at both roller/profile and bush/roller interfaces. For this case, no kinematic condition constrains roller rotation. It is therefore assumed that no rolling occurs at the bush/roller interface (Fig. 17).

As a consequence, the roller/profile contact point slides a distance Δs_k. Fig. 17 illustrates this change of orientation, the roller in sub-position k is represented by a dotted line while sub-position $k+1$ by a solid line. Excluding any unlikely self-rotation of the roller, this corresponds to the kinematic condition with the longest sliding distance. For case B, the roller rotation is expressed as follows.

$$\Delta\theta_k = \frac{\Delta s_k}{R_{curve}} \tag{19}$$

with: R_{curve} the profile curvature radius at the roller/profile contact point considered. It can be positive or negative depending on whether the profile portion considered is convex or concave, respectively.

Cases A and B represent two extreme kinematic conditions: in case A, the sliding distance at the roller/profile contact point is null while it is maximal for case B (excluding roller self-rotation). For case B, sliding is assumed at both roller interfaces. Following Coulomb friction theory, the tangential force is therefore fixed at both interfaces and roller equilibrium cannot be achieved. However, no feedback loop is considered in the chain drive model between kinematics and loads. The roller kinematics as given by the chain drive model is therefore considered to be independent of any later assumption regarding kinematics (case A or B) or loads.

Between sub-position k and $k+1$, link tensions and roller/profile contact force are considered as constant. The values $\overline{P}_k$, $\overline{T}_{i+1}^{(k)}$ and $\overline{T}_i^{(k)}$ are assumed to be the mean between position k and $k+1$.

Assuming Coulomb friction with sliding at a given interface [44], the magnitudes of tangential and normal forces ($\mathbf{F_T}$and $\mathbf{F_N}$, respectively) are linked by the friction coefficient μ (Eq. 19).

$$\| \mathbf{F_T} \| = \mu \| \mathbf{F_N} \| \tag{20}$$

With μ sliding friction coefficient at the interface considered.

This equation can be rearranged using the total force $\mathbf{F}$ as follows.

$$\| \mathbf{F_T} \| = \frac{\mu}{\sqrt{1+\mu^2}} \| \mathbf{F} \| \tag{21}$$

Returning to our application, T and P are magnitudes of total forces $\| \mathbf{F} \|$. Therefore, the magnitudes of the forces producing work at each interface are given in Table 1: Magnitudes of tangential force at each interface for pin and bush articulations according to Eq. (21). with: μ_{pb}, μ_{br} and μ_{rp} friction coefficient at pin/bush, bush/roller and roller/profile interface, respectively.

Contact force P applies at the roller/profile interface. As dynamical effects are neglected, the bush/roller force also has a magnitude of P. For the bin/bush interface, the force to be considered is the tension in the neighbouring pin link. It therefore depends on the articulation being a pin or a bush one. For a pin articulation, $T_i^{(k)}$ is considered while $T_{i+1}^{(k)}$ is used for a bush one (see Table 1).

3.2. Articulation definition

3.2.1. Pin articulation

Fig. 18 shows motion parameters (*i.e.*, ν, κ, α^* and θ) and forces (T_i, T_{i+1} and P_i) on a pin articulation. The preceding link is a pin link (tension $T_i^{(k)}$, orientation κ) and the following one is a bush link (tension $T_{i+1}^{(k)}$ and orientation ν).

The losses undergone by a pin articulation are split into the contribution of each interface: pin/bush, bush/roller and roller/profile. The developments are presented below for the pin/bush interface (pb) example.

The dissipated work at a given interface is calculated considering the product between the sliding distance and the tangential force (Table 1). Between sub-positions k and k+1, the pin/bush interface is subject to the following sliding distance.

Table 1
Magnitudes of tangential force at each interface for pin and bush articulations.

Interface	Pin articulation	Bush articulation
Pin/bush	$\overline{T}_{i+1}^{(k)} \frac{\mu_{pb}}{\sqrt{1+\mu_{pb}^2}}$	$\overline{T}_i^{(k)} \frac{\mu_{pb}}{\sqrt{1+\mu_{pb}^2}}$
Bush/roller	$\overline{P}^{(k)} \frac{\mu_{br}}{\sqrt{1+\mu_{br}^2}}$	
Roller/profile	$\overline{P}^{(k)} \frac{\mu_{rp}}{\sqrt{1+\mu_{rp}^2}}$	

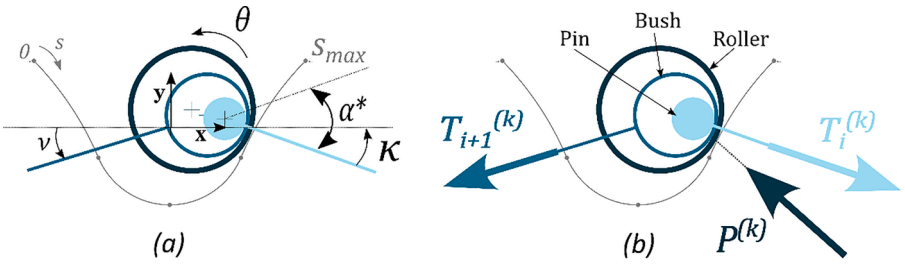

Fig. 18. (a) motion parameters and (b) forces on pin articulations.

$$d_{sliding}\big|^{(k)}_{pb,pin\_art} = R_{pin}\left|\Delta\alpha^{*(k)}\right| \tag{22}$$

This motion occurs under the following tangential force.

$$F_T\big|^{(k)}_{pb,pin\_art} = \overline{T}_i^{(k)}\frac{\mu_{pb}}{\sqrt{1+\mu_{pb}^2}} \tag{23}$$

The resulting work is then expressed as follows.

$$\begin{aligned} W\big|^{(k)}_{pb,pin\_art} &= d_{sliding}\big|^{(k)}_{pb,pin\_art} F_T\Big|^{(k)}_{pb,pin\_art} \\ &= R_{pin}\left|\Delta\alpha^{*(k)}\right|\overline{T}_i^{(k)}\frac{\mu_{pb}}{\sqrt{1+\mu_{pb}^2}} \end{aligned} \tag{24}$$

Finally, the total work dissipated at the pin/bush interface during the contact with the sprocket (sprocket j) considered is obtained by summing Eq. (24) from the sub-position of roller capture ($k = 1$) to the sub-position of roller release ($k = k_{\max}$).

$$\begin{aligned} W\big|^{j}_{pb,pin\_art} &= \sum_{k=1}^{k_{\max}-1} W\big|^{(k)}_{pb,pin\_art} \\ &= \sum \overline{T}_i^{(k)}\frac{\mu_{pb}}{\sqrt{1+\mu_{pb}^2}} R_{pin}\left|\Delta\alpha^{*(k)}\right| \end{aligned} \tag{25}$$

3.2.2. Summary of dissipated work

Sliding distance and load at each articulation interface are summarised in Table 2.

Dissipated works at each articulation interface are summarised in Table 3.

3.3. Drive dissipation

The results of the mechanical work dissipated at each articulation is then combined to calculate the efficiency of the drive. Losses are considered only during the contact with sprockets. Therefore, during an entire drive rotation, a pin articulation undergoes the following dissipation ($j = I$ and II for the chainring and rear cog, respectively).

$$W_{pin\_art} = \sum_{j=I}^{j=II} W^j_{pin\_art} \tag{26}$$

Similarly, the work dissipated by a bush articulation is given by Eq. (27).

Table 2
Dissipated work at each interface.

Interface		Pin articulation	Bush articulation
Pin/bush	Sliding Distance	$R_{pin}\left\|\Delta\alpha^{*(k)}\right\|$	
	Load	$\overline{T}_i^{(k)}$	$\overline{T}_{i+1}^{(k)}$
Bush/Profile	Sliding Distance	$R_{bush}\left\|\Delta\theta^{(k)} - \Delta\nu^{(k)}\right\|$	$R_{bush}\left\|\Delta\theta^{(k)} - \Delta\kappa^{(k)}\right\|$
	Load	$\overline{P}_i^{(k)}$	
Roller/Profile	Sliding Distance	Case A: 0 case B: $\Delta s^{(k)}$	
	Load	$\overline{P}_i^{(k)}$	

Table 3
Work dissipated in each chain articulation interface between sub-positions k and k+1.

Interface		Pin articulation	Bush articulation
Pin/bush		$T_i^{(k)}\frac{\mu_{pb}}{\sqrt{1+\mu_{pb}^2}}R_{pin}\left\|\Delta\alpha_k^*\right\|$	$T_{i+1}^{(k)}\frac{\mu_{pb}}{\sqrt{1+\mu_{pb}^2}}R_{pin}\left\|\Delta\alpha_k^*\right\|$
Bush/roller	*Case A*	$\overline{P}_i^{(k)}\frac{\mu_{br}}{\sqrt{1+\mu_{br}^2}}R_{bush}\left\|\frac{-\Delta s_k}{R_{roller}}-\Delta\nu_k\right\|$	$\overline{P}_i^{(k)}\frac{\mu_{br}}{\sqrt{1+\mu_{br}^2}}R_{bush}\left\|\frac{-\Delta s_k}{R_{roller}}-\Delta\kappa_k\right\|$
	Case B	$\overline{P}_i^{(k)}\frac{\mu_{br}}{\sqrt{1+\mu_{br}^2}}R_{bush}\left\|\frac{\Delta s_k}{R_{curve}}-\Delta\nu_k\right\|$	$\overline{P}_i^{(k)}\frac{\mu_{br}}{\sqrt{1+\mu_{br}^2}}R_{bush}\left\|\frac{\Delta s_k}{R_{curve}}-\Delta\kappa_k\right\|$
Roller/profile	*Case A*	0	
	Case B	$\overline{P}_i^{(k)}\frac{\mu_{rp}}{\sqrt{1+\mu_{rp}^2}}\Delta s_k$	

$$W_{bush\_art}=\sum_{j=I}^{j=II}W_{bush\_art}^{j} \tag{27}$$

For a complete rotation of the drive, the total work dissipated by all the chain articulation is as follows.

$$W_{tot}=\frac{N_{link}}{2}\left(W_{pin\_art}+W_{bush\_art}\right) \tag{28}$$

With N_{link} the total chain number of links.N_{link} is always an even number as cranked links are not studied in this work. This amount of work is dissipated within a time Δt required for a complete drive rotation (see Eq. (29)).

$$\Delta t=\frac{N_{link}}{Z_I}\frac{2\pi}{\Omega_I} \tag{29}$$

With Ω_I the chainring rotational speed rad/s (given as input).
Therefore, the total power loss caused by the dissipation in all the chain articulations is given as follows.

$$P_{loss}=\frac{W_{tot}}{\Delta t} \tag{30}$$

The energy efficiency of the drive is therefore:

$$\eta=1-\frac{P_{loss}}{C_I Z_I} \tag{31}$$

With C_I the mean chainring torque (over full drive rotation).

The dissipated works depend on the kinematic case considered (case A or B). Therefore, using Eq. (31), two efficiency values η_A and η_B are obtained, one for each kinematic case. Case B (sliding at both bush/roller and roller/profile interfaces) is the less favourable in terms of chain drive efficiency and therefore η_B is always the lower bound of the interval.

The chain drive model introduced in this paper is quasi static. Therefore, its results are independent of the drive rotational speed. The work dissipated in a chain articulation is calculated based on these speed free results. No notion of speed is added in the calculation of the dissipated work (see Table 2: Dissipated work at each interface, friction coefficients are assumed to be constant). The drive rotational speed appears in Eq. (30) giving the power loss but cancels in Eq. (31). In this model, the drive efficiency η is therefore independent from any speed consideration. This consequence of the quasi static chain drive model is supported by the experimental results of Lodge & Burgess [35] showing no significant effect of the rotational speed on efficiency. These tests were run for moderate speeds (up 150*rpm*) which is consistent with track cycling applications. For higher rotational speeds, the effect on power losses could be considered, for instance, by adding a physical model for the calculation of friction coefficients (presented for instance in [45]). However, such a model was not used in this work.

4. Elements of validation

The predictions of the Chain Drive Efficiency Model (CDEM) are compared to the work presented by Lodge & Burgess in [35]. In their paper, a model of chain drive efficiency was proposed considering only meshing losses at both the tight and slack strands. Experimental measurements were also conducted at several rotational speeds and used to validate the model. This comparison focusses on a 19|19 chain drive. It is specified in the paper that a Renold BS [2] chain of pitch 1/2'' with 100 links was used but the tension setup and the tooth profile used were not mentioned. To allow the comparison, the CDEM is set with the parameters given in Table 4**.** The friction correction angle is $|\delta(\infty)|=5^{\circ}$ and the slack strand looseness is set at slack=7.25% (details about this tension setting are given below). The chain characteristics are summarised in Table 5 according to the manufacturer's catalogue [2] for a BS chain of 1/2''. In addition, pin and bush diameters (not given in the catalogue) were measured on an ISO industrial chain of matching pitch. All the friction coefficients μ_{pb}, μ_{br} and μ_{rp} are assumed to be constant and Eq.ual to 0.11, as given in the paper for a lubricated steel/steel contact [36].

Table 4
Drive parameters for comparison with Lodge & Burgess [35].

$Z_I \vert Z_{II}$	L	ΔY	slack	$\vert\delta(\infty)\vert$
19|19	513.7mm	0	7.25%	5°

Table 5
Chain parameters from [2] for comparison with Lodge & Burgess [35].

Pitch p	D_{pin}	D_{bush}	D_{roller}	m_{link}
12.7mm	4.42mm	6.37mm	8.51mm	8.89g

It can be noted that the chain used is significantly heavier than a bicycle chain. The Renold BS chain has a mass of $8.89g\ /link$, heavier than regular track cycling chains. This choice was made on purpose in the paper to favour losses in the slack strand (heavier links increase the slack strand tension).

In order to ensure comparison with the efficiency model presented by Lodge & Burgess [35], losses due to meshing had to be distinguished from the roller ones. Losses due to meshing are calculated considering only the losses occurring during the meshing and un-meshing period. Knowing the CDEM meshing losses, the looseness setting *slack* is chosen so that CDEM meshing loss predictions equal those of Lodge & Burgess's model for $C_{II} = 30N.m$ (*i.e.*, to fit the prediction of both models for the biggest torque, see Fig. 19). The value obtained (slack=7.25%) is higher than the 4 to 6% recommended from industrial drive [40] but still represents a realistic tension setting. The corresponding slack strand tension varies around 14.5N.

Fig. 19 shows the comparison between the efficiency model of Lodge & Burgess, the experimental measurements performed by Lodge & Burgess, and the CDEM. The meshing losses, calculated as detailed above, are also shown. The interval between the two extreme efficiencies η_A and η_B is represented in the shaded area. As mentioned, case B corresponds to the lower efficiency.

Both CDEM meshing losses and the model of Lodge & Burgess predict the same increase in chain drive efficiency with increasing output torques C_{II}. Considering only the meshing losses, this effect is explained as follows. The input power and the tight strand tension increase with torque. In the meantime, the slack strand tension remains the same (global kinematics is independent of the loading conditions). Therefore, the significance of the slack strand meshing losses decreases as torque increases, resulting in growing efficiency. Compared to the model of Lodge & Burgess, the whole CDEM (shaded area in Fig. 19) exhibits lower efficiency due to additional roller losses. The effect of roller losses is particularly significant for low torque. For instance, for $C_{II} = 1N.m$, the efficiency predicted considering only meshing losses is about 97% while the full CDEM predicts down to 94.1% (for case B) considering the effect of roller losses. This is consistent with the fact that case B assumes sliding at both interfaces (bush-roller and roller profile), which makes it less favourable than case A (slippage only at the bush-roller interface) and therefore less favourable in terms of chain drive efficiency. However, with increasing torque, the effect of roller losses decreases as the predicted interval tends toward the meshing losses curve. Compared to the experimental measurements, Lodge & Burgess's efficiency model mostly overestimates the drive efficiency, especially for low torques. This overestimation was attributed in the paper [35] to vibrations and roller sprocket impacts. The

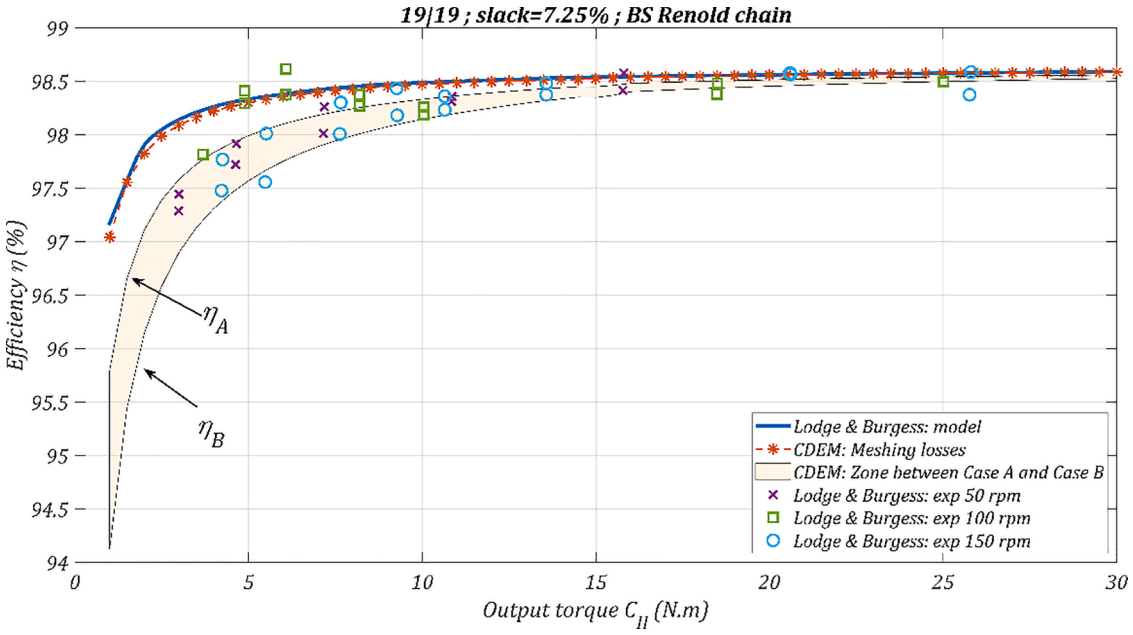

Fig. 19. Chain drive efficiency, comparison with Lodge & Burgess [35].

CDEM shows better agreement with the experimental results. Indeed, the lower efficiency, due to roller losses, is in accordance with the experimental measurements at low torques. This result suggests that the losses responsible for the deviation of Lodge & Burgess's model from the experimental results could be caused by roller motion. It should be noted that the agreement with the measurements made at 100 rpm is less convincing. The experimental efficiencies are higher than those observed for the 50 and 150 rpm cases at low torque, which is not represented by the model. However, the quasi-static model takes into account the variation in torque but neglects the effect of rotation speed (inertia, vibrations, etc.). The increase in efficiency at 100 rpm and low torque could suggest a specific influence of rotational speed and remains outside the scope of the quasi-static model. Despite this, the good agreement with the experimental results and the absence of a clear trend with increasing speed suggest that the rotational speed of the drive is not a first-order parameter on efficiency.

5. Conclusions

The Chain Drive Efficiency Model (CDEM) was introduced. This 2D model studies a chain drive considering the connections between strands and sprockets, each represented by specific sub-model. The local sub-model used for the sprockets was detailed. It is used to calculate the loads (*i.e.*, link tension and roller/profile contact force) and roller locations along their corresponding tooth profile simultaneously, as both are intertwined. The general solving procedure for the whole model was then introduced. The global kinematics was solved first before its results were used in the local sprocket sub-model. The external loading conditions can be prescribed *via* a torque applied on either sprockets or *via* the tight strand tension. This sequential approach facilitates the solution of each sub-model but introduces compatibility issues.

The efficiency is calculated considering meshing losses and losses due to roller motions along their corresponding tooth profile. The efficiency model considers all losses due to friction at the chain interfaces. This includes meshing losses and losses caused by roller motion along their associated tooth profile. The chain is assumed to be perfectly aligned and therefore friction is considered only at the pin/bush, bush/roller and roller/profile interfaces (no lateral contact occurs with plates). Coulomb friction is assumed at all interfaces. Differences between pin and bush articulations are considered. Additional kinematic hypotheses are stated to determine roller rotation. Two extreme cases, meant to represent the best and worst possible conditions, were considered. As a consequence of the two kinematic cases considered, the predicted efficiency is given in the form of an interval $[\eta_B, \eta_A]$.

The CDEM predictions were then compared to results from the literature. Predictions agreed with the experimental measurements of Lodge & Burgess [35] for an industrial drive. The results showed that lower efficiencies observed at low torque, which could not be explained by a model considering only meshing losses, seemed to be due to roller motion losses. This comparison demonstrates the interest of the model presented with respect to its predecessors.

Further work will include validation against an experimental device built for track cycling applications. The CDEM will then be used to explore the effectiveness of track cycling training and identify potential improvements in the various training parameters. This new approach, based on a global kinematic model and on the local movement of the rollers, will make it possible to add an in-depth analysis of the influence of global parameters (applied torque, tension, pinion size in terms of number of teeth and pitch size) as well as local parameters (tooth profile, lubrication coefficient, etc.). Because of the number of parameters, a special study will be carried out to determine which are of prime importance and which must be optimised if the athlete is to win the race.

The link between global and local kinematics must also be questioned. In the CDEM, the general positioning of the rollers is on the pitch circle of the pinion and it is assumed that this position remains identical regardless of the load. In the case of a heavily loaded gear (sprint start for example), this assumption may be called into question because the strong forces applied to the rollers could then affect their position. If the experimental validation and study of the parameters points in this direction, a strong link will have to be put in place to calculate the general positioning of the roller in relation to the load it is subjected to. Once the model has been validated for all race conditions, a dynamic model capable of taking into account the influence of inertia and vibration, particularly over a full race during which the transmission load varies, would be useful for research into the efficiency of track cycling transmissions.

CRediT authorship contribution statement

G. Lanaspeze: Formal analysis, Methodology, Conceptualization, Resources, Software, Visualization, Validation, Writing – original draft, Writing – review & editing. **B. Guilbert:** Formal analysis, Methodology, Investigation, Data curation, Conceptualization, Supervision, Validation, Writing – review & editing. **L. Manin:** Supervision, Methodology, Investigation, Funding acquisition, Conceptualization. **F. Ville:** Project administration, Investigation, Writing – review & editing, Validation, Supervision, Methodology, Data curation, Conceptualization, Formal analysis.

Declaration of competing interest

The authors declare that they have no known competing financial interests or personal relationships that could have appeared to influence the work reported in this paper.

Data availability

Data will be made available on request.

Acknowledgements

This work is founded by INSA Lyon and is part of the THPCA2024 project supported by ANR (Grant No. ANR-2020-STHP2-000). The authors thank Jérôme CAVORET and Martin BEST for their relevant remarks and ideas during the conception of this studies. The authors would also like to thank Jean-Christophe PERAUD for is support during the study as part of the THPCA2024 project.

Appendix

a. Calculation of the mid-span movement

It is assumed that the maximal slack strand deflection is obtained when the slack strand trajectory is constrained in such way that it forms two straight parts connected at the link where the hypothetic load is applied (see Fig. 20). Therefore, for each roller of the slack strand, the corresponding two lines trajectory is computed by finding the intersection of two circles:

- Circle of centre E_I and radius $i_{ms}.p$
- Circle of centre E_{II} and radius $(n_s - i_{ms}).p$

with: $i_{ms} \in 1, n_s - 1$

Note: Index i_{ms} is different from the spatial index i used for rollers and links numbering.

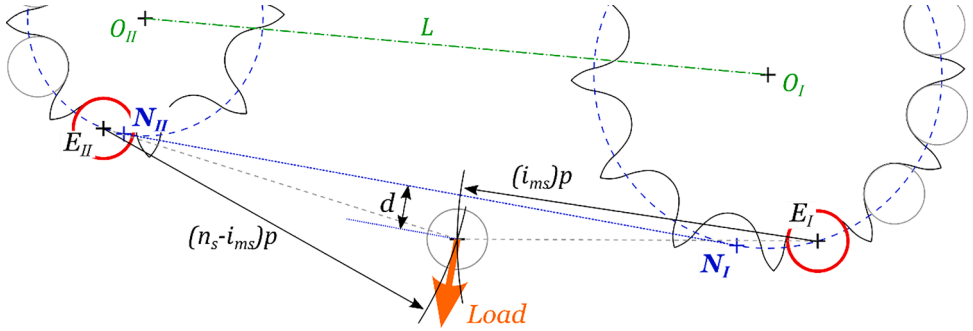

Fig. 20. Calculation of the mid-span movement $d = \max(d_{i_{ms}})$.

Once the intersection point is found, the distance $d_{i_{ms}}$ of each roller i_{ms} to the common tangent is calculated. The process is repeated for all i_{ms}. The mid-span movement for sub-position m is considered to be twice the biggest found deflection $d = \max(d_{i_{ms}})$ (Fig. 20). This leads to Eq. (32) giving the expression of the instantaneous $slack_m$ parameter (*i.e.*, for a given drive sub-position m). The final *slack* is calculated as a mean for ten linearly spaced sub-positions.

$$slack_m = \frac{2d}{L} \tag{32}$$

It must be noted that this geometric method does not consider possible collision between the stretched strand and the sprockets. Indeed, for high looseness, a slack strand stretched upward might collide a sprocket. For such case, the theoretical two-line trajectory, assumed for mid-span calculation cannot be reached (see Fig. 21). The theoretical mid-span movement would therefore be higher than what could be measured for a real drives in identical conditions. Moreover, the calculated geometric deflection is the limit theoretically obtained for an infinite force pulling the strand. The deflection observed on a real drive would necessarily be smaller.

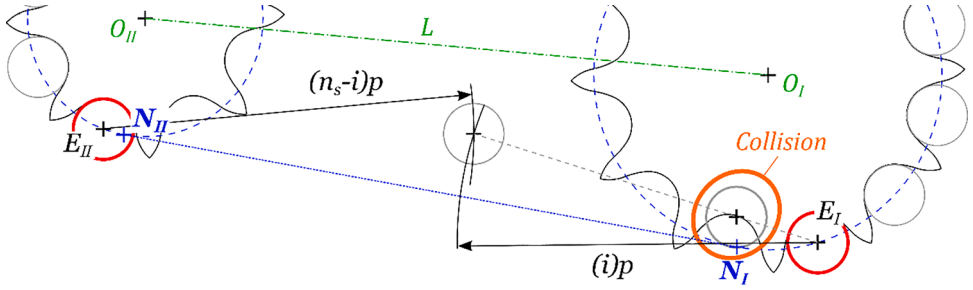

Fig. 21. Possible collision between the stretched slack strand and the sprockets.

b. Choice of a (transition of friction correction parameter)

The tanh function is introduced to calculate the friction correction angle δ. It allows to continuously join the two extreme values $\pm\text{atan}(\mu_\delta)$. The tanh function depends on the parameter a giving the width of the transition zone. The choice of this parameter changes the relation between δ and $s_{c,1}$ (see Eq. (13)) therefore influencing the relation between $s_{c,1}$ and the loading conditions. a is a numerical parameter, therefore, its value is chosen so that it does not influence the results obtained.

Due to the connection between the global kinematics (which considers all the roller centres on the pitch circles) and the local sprocket sub-model (considering precise roller location along the tooth profile), the slack strand tensions $T_{s,j}$ change discontinuously when a roller is added or removed to the slack strand. These discontinuities pass from the slack tension to the tension ratio applied on the sprockets. Combined with the modification of δ, these discontinuities can be amplified resulting in significant jumps in the roller location evolution predicted. Depending on the value of a, the amplitude of these discontinuities varies (see evolution of s_c in Fig. 22).

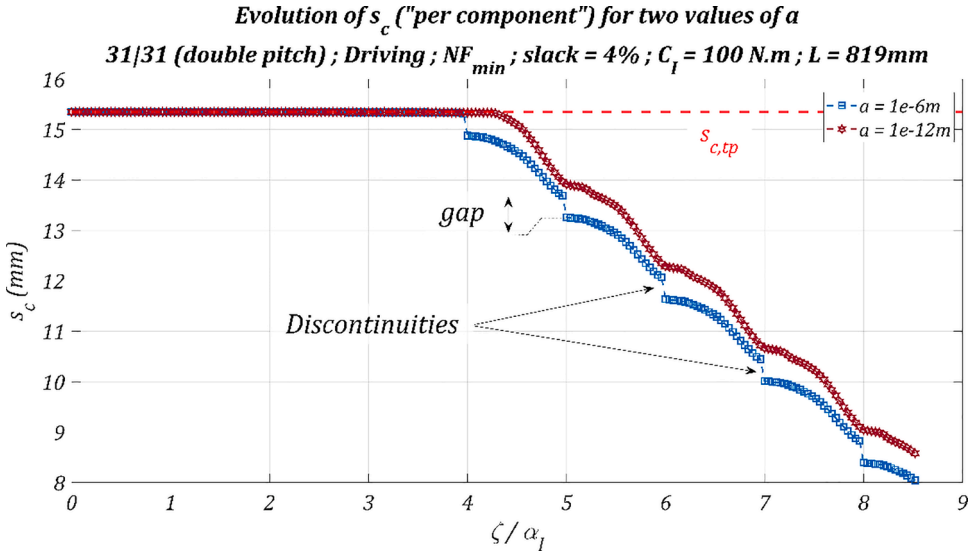

Fig. 22. Examples of discontinuities in s_c evolution for the driving sprocket.

The value of a is chosen so that it does not affect the amplitude of the discontinuities. Fig. 23 shows the maximal gap (defined in Fig. 22) on the roller location s_c depending on the torque applied on the driving sprocket for several values of a (from $a = 1e^{-6}m$ to $a = 1e^{-12}m$). Two drives are studied, a 31|31 double pitch industrial drive ($slack = 4\%$) and a 60|15 cycling drive ($slack = 11\%$), both with the same tooth profile. All calculations are performed with $|\delta(\infty)| = 5°$.

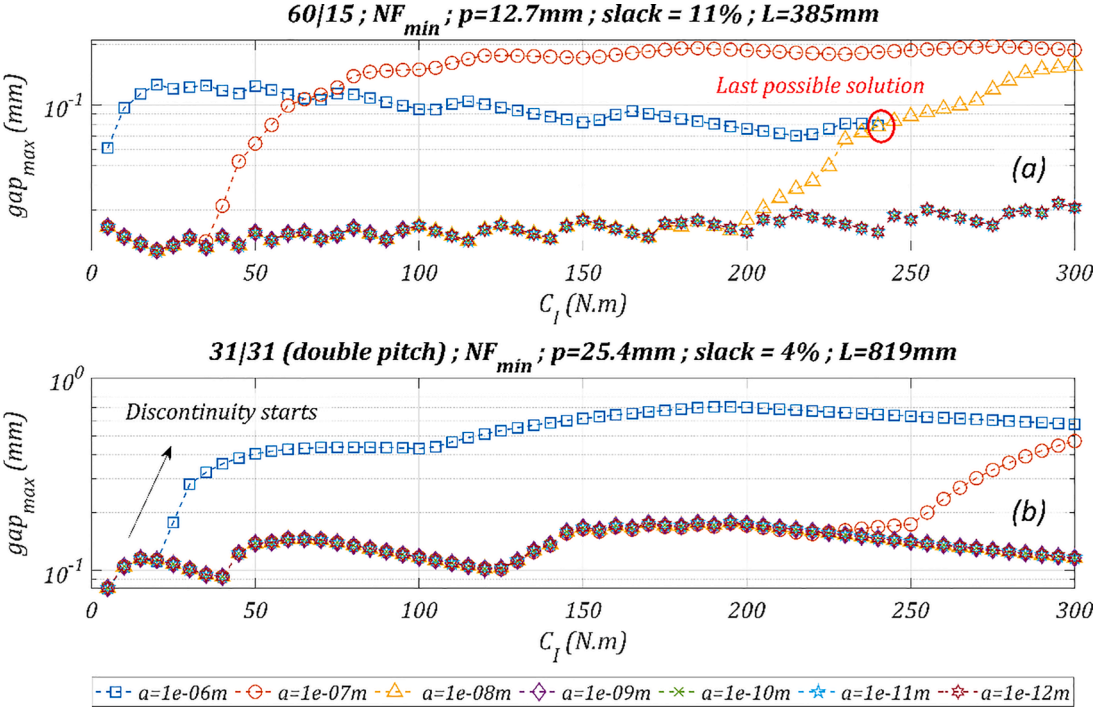

Fig. 23. Evolution of the maximal gap depending on parameter a for identical tooth profiles with (a) cycling (60|15, p=12.7mm, slack=11% and L=385mm) (b) industrial drives (31|31-double pitch, p=25.4mm, slack=4% and L=819mm).

For the cycling drive (Fig. 23.a), the $a = 1e^{-6}m$ curve stops at $C_I = 240N.m$ as no solution was found beyond (*i.e.*, the value of a also

influences the limit tension ratio). Emergence of discontinuities are characterised by rapid increase of the gap. For both cases, large values of a induce the apparition of discontinuities. For the industrial drive (Fig. 23.b), no effect is reported for value smaller than $1e^{-7}m$ (for the explored torque range), $1e^{-8}$ for the cycling drive.

The influence of the parameter a varies depending on the profile used and the loading conditions. Therefore, to be sure to always lie on the plateau where variable a has no effect, a value of $a = 1e^{-10}m$ is chosen for all the paper calculations (unless otherwise stated).

References

[1] L. Da Vinci, *Codex Atlanticus*, 1478, 1119 p.
[2] B. Tripp, Renold Chains: A history of the company and the rise of the precision chain industry 1879-1955, Taylor & Francis, 2006, p. 191.
[3] R. Tandler, N. Bohn, U. Gabbert, E. Woschke, Experimental investigations of the internal friction in automotive bush chain drive systems, Tribol. Int. 140 (July) (2019) 105871, https://doi.org/10.1016/j.triboint.2019.105871.
[4] R. Tandler, N. Bohn, U. Gabbert, E. Woschke, Analytical wear model and its application for the wear simulation in automotive bush chain drive systems, Wear 446-447 (January) (2020) 203193, https://doi.org/10.1016/j.wear.2020.203193.
[5] C.U. Kim, J.Y. Chung, J. Il Song, Dynamic analysis of long heavy-duty roller chain for bucket elevator of continuous ship unloader, Adv. Mech. Eng. 9 (8) (2017) 1–11, https://doi.org/10.1177/1687814017723296.
[6] X. Ma, X. Shi, J. Zhang, Modeling and experimental investigation on the vibration of main drive chain in escalator," *INTER-NOISE 2019 MADRID - 48th Int*, Congr. Exhib. Noise Control Eng. (2019).
[7] B. Kohler, E. Sztrygler, Chaînes mécaniques, Fonct. Compos. Mécaniques (1989) 41, https://doi.org/10.51257/a-v1-b5650, vol. base docum, no. ref. article : b5650.
[8] R.C. Binder, Mechanics of the Roller Chain Drive: Based on Mathematical Studies by R. C. Binder, Prentice-Hall, 1956, p. 204.
[9] S. Mahalingam, Polygonal action in chain drives, J. Franklin Inst. 265 (1) (1958) 23–28, https://doi.org/10.1016/0016-0032(58)90665-3.
[10] R.A. Morrison, Polygonal action in roller chain drives, Mach. Des. (1952) 155–159.
[11] G. Bouillon, G.V. Tordion, On polygonal action in roller chain drives, J. Manuf. Sci. Eng. Trans. ASME 87 (2) (1965) 243–251, https://doi.org/10.1115/1.3670804.
[12] N. Fuglede, J.J. Thomsen, Kinematics of roller chain drives - Exact and approximate analysis, Mech. Mach. Theory 100 (2016) 17–32, https://doi.org/10.1016/j.mechmachtheory.2016.01.009.
[13] N. Fuglede, Kinematics and Dynamics of Roller Chain Drives, Technical University of Denmark, 2014, p. 200. Thesis.
[14] M.R. Naji, K.M. Marshek, Analysis of sprocket load distribution, Mech. Mach. Theory 18 (5) (1983) 349–356, https://doi.org/10.1016/0094-114X(83)90130-1.
[15] M.R. Naji, K.M. Marshek, Experimental determination of the roller chain load distribution, J. Mech. Des. Trans. ASME 105 (3) (1983) 331–338, https://doi.org/10.1115/1.3267365.
[16] B.H. Eldiwany, K.M. Marshek, Experimental load distributions for double pitch steel roller chains on polymer sprockets, Mech. Mach. Theory 24 (5) (1989) 335–349, https://doi.org/10.1016/0094-114X(89)90064-5.
[17] M.R. Naji, K.M. Marshek, Analysis of roller chain sprocket pressure angles, Mech. Mach. Theory 19 (2) (1984) 197–203, https://doi.org/10.1016/0094-114X(84)90042-9.
[18] M.R. Naji, K.M. Marshek, The effects of the pitch difference on the load distribution of a roller chain drive, Mech. Mach. Theory 24 (5) (1989) 351–362, https://doi.org/10.1016/0094-114X(89)90065-7.
[19] N.E. Hollingworth, D.A. Hills, Theoretical efficiency of a cranked link chain drive, Proc. Inst. Mech. Eng. Part C J. Mech. Eng. Sci. 200 (5) (1986) 375–377, https://doi.org/10.1243/PIME_PROC_1986_200_141_02.
[20] N.E. Hollingworth, D.A. Hills, Forces in a heavy-duty drive chain during articulation, Proc. Inst. Mech. Eng. Part C J. Mech. Eng. Sci. 200 (5) (1986) 367–374, https://doi.org/10.1243/PIME_PROC_1986_200_140_02.
[21] M.S. Kim, G.E. Johnson, Mechanics of roller chain-sprocket contact: a general modelling stragegy. American Society of Mechanical Engineers, Design Engineering Division (Publication) DE, 1992, pp. 689–695, 43 pt 2.
[22] T. Verne, "Simulation et analyse du comportement des transmissions par chaine à rouleaux",Thèse, INSA Lyon,1994.
[23] I. Troedsson, L. Vedmar, A method to determine the static load distribution in a chain drive, J. Mech. Des. Trans. ASME 121 (3) (1999) 402–408, https://doi.org/10.1115/1.2829475.
[24] I. Troedsson, L. Vedmar, A method to determine the dynamic load distribution in a chain drive, Proc. Inst. Mech. Eng. Part C J. Mech. Eng. Sci. 215 (5) (2001) 569–579, https://doi.org/10.1243/0954406011520959.
[25] I. Troedsson, L. Vedmar, A method to determine the static load distribution in a chain drive, Proc. Inst. Mech. Eng. Part C J. Mech. Eng. Sci. 215 (5) (2001) 569–579, https://doi.org/10.1243/0954406011520959.
[26] M.S. Kim, G.E. Johnson, Mechanics of roller chain-sprocket contact: a general modelling stragegy. American Society of Mechanical Engineers, Design Engineering Division (Publication) DE, 1992, pp. 689–695, vol. 43 pt 2.
[27] S.L. Pedersen, Simulation and Analysis of Roller Chain Drive Systems, Technical University od Denmark (DTU), 2004.
[28] H. Zheng, Y.Y. Wang, K.P. Quek, A refined numerical simulation on dynamic behavior of roller chain drives, Shock Vib. 11 (5–6) (2004) 573–584, https://doi.org/10.1155/2004/548172.
[29] G. Hippmann, M. Arnold, M. Schittenhelm, D C, Simulation, "efficient simulation of bush and roller chain drives," Multibody Dyn. 2005, ECCOMAS Themat. Conf. (June) (2005) 21–24.
[30] C. Pereira, J. Ambrosio, A. Ramalho, Contact mechanics in a roller chain drive using a multibody approach, 11th Pan-Am. Congr. Appl. Mech. (1994) (2010).
[31] J. Ambrosio, C. Malça, A. Ramalho, Planar roller chain drive dynamics using a cylindrical contact force model, Mech. Based Des. Struct. Mach. 44 (1–2) (Apr. 2016) 109–122, https://doi.org/10.1080/15397734.2015.1087319.
[32] M. Omar, Multibody dynamics formulation for modeling and simulation of roller chain using spatial operator, in: MATEC Web of Conferences 51, 2016, https://doi.org/10.1051/matecconf/20165101003.
[33] M.A. Omar, Chain drive simulation using spatial multibody dynamics, Adv. Mech. Eng. 2014 (2014), https://doi.org/10.1155/2014/378030.
[34] M.D. Kidd, N.E. Loch, R.L. Reuben, Bicycle chain efficiency, Heriot-Watt University, Scotland, 2000, https://doi.org/10.1201/9781003078098-37.
[35] C.J. Lodge, S.C. Burgess, A model of the tension and transmission efficiency of a bush roller chain, Proc. Inst. Mech. Eng. Part C J. Mech. Eng. Sci. 216 (4) (2002) 385–394, https://doi.org/10.1243/0954406021525179.
[36] C.J. Lodge, Theoretical and experimental studies of the mechanical behaviour of roller chains, University of Bristol, 2002, https://doi.org/10.1088/1361-6404/ac2881.
[37] C.J. Lodge, S.C. Burgess, An investigation into the selection of optimum chain and sprocket size, J. Eng. Des. 15 (6) (2004) 563–580, https://doi.org/10.1080/09544820410001731128.
[38] J.B. Spicer, C.J.K. Richardson, M.J. Ehrlich, J.R. Bernstein, M. Fukuda, M. Terada, Effects of frictional loss on bicycle chain drive efficiency, J. Mech. Des. Trans. ASME 123 (4) (2001) 598–605, https://doi.org/10.1115/1.1412848.
[39] G. Lanaspeze, B. Guilbert, L. Manin, F. Ville, Preliminary modelling of power losses in roller chain drive: application to single speed cycling, Mech. Ind. 23 (2022) 27, https://doi.org/10.1051/meca/2022026.

[40] Diamond Chain Company, "Technical Engineering", *Diamond katalog glowny lancuchy,* 2004, 177 p.
[41] A. Bodin, L. Blanc-Centi, N. Borne, B. Boutin, L. Desideri, D. Mégy, P. Romon, *Géométrie – Quelques chapitres de géométrie,* 2016, 154 *p*.
[42] M.R. Naji, K.M. Marshek, The effects of the pitch difference on the load distribution of a roller chain drive, Mech. Mach. Theory 24 (5) (1989) 351–362, https://doi.org/10.1016/0094-114X(89)90065-7.
[43] M.R. Naji, K.M. Marshek, Experimental determination of the roller chain load distribution, J. Mech. Des. Trans. ASME 105 (3) (1983) 331–338, https://doi.org/10.1115/1.3267365.
[44] E. Popova, V.L. Popov, The research works of Coulomb and Amontons and generalized laws of friction, Friction 3 (2) (2015) 183–190, https://doi.org/10.1007/s40544-015-0074-6.
[45] Y. Diab, F. Ville, P. Velex, Prediction of power losses due to tooth friction in gears, Tribol. Trans. 49 (2) (2006) 260–270, https://doi.org/10.1080/05698190600614874.